2013

Projectile Fire-Control Algorithm in a Spatially Varying Wind Field

Lakmal Kaviratna
Georgia Institute of Technology - Main Campus

Mark Costello
Georgia Institute of Technology - Main Campus

Nathan Slegers
George Fox University, nslegers@georgefox.edu

Projectile Fire-Control Algorithm in a Spatially Varying Wind Field

Lakmal Kaviratna* and Mark Costello†
Georgia Institute of Technology, Atlanta, Georgia 30332
and
Nathan Slegers‡
University of Alabama in Huntsville, Huntsville, Alabama 35899

The fire-control solution is an important element of any modern weapon system, providing precise aiming of the gun to enable highly accurate projectile impact. To be practical, the fire-control solution must be computed rapidly and reliably while simultaneously including all pertinent physical effects that can alter the trajectory and impact point. Current fire-control solutions account for the effect of atmospheric wind in a rudimentary manner, typically assuming a constant crosswind that is estimated in the field or measured at the firing site. With the advent of advanced wind-measurement systems (light detection and ranging, for example), it is now possible to accurately measure three-dimensional wind velocities at numerous points approximately along the path of a direct-fire projectile. This article first shows the importance of wind knowledge along the line of fire for accuracy, particularly for long-range direct-fire shots. Then, a method to compute the fire-control solution of a projectile is defined, including the effect of exactly known spatially varying winds. By using a modified form of projectile linear theory that incorporates three-dimensional linearly varying atmospheric winds, a closed-form fire-control solution is obtained. Moreover, the solution can be rapidly computed. The key to the algorithm is partitioning the projectile linear-theory state-transition matrix in an input–output form that enables the aiming solution to be computed in terms of a desired impact point and measured atmospheric winds. The application of this algorithm is restricted to flat-fire trajectories where the angle of attack of the projectile remains low throughout because this is the key limitation of the projectile linear theory that must be maintained. The proposed algorithm is exercised on an example fire-control problem for such flat-fire trajectories with excellent results.

Nomenclature

C_{x0}	=	projectile aerodynamic body x-axis force coefficient
C_{LDD}	=	projectile roll moment coefficient due to fin cant per fin cant angle
C_{LP}, C_{MQ}, C_{NR}	=	projectile roll, pitch, and yaw damping coefficients
C_{NA}	=	projectile yaw moment coefficient slope with respect to angle of attack
C_{YPA}	=	projectile Magnus force coefficient slope with respect to angle of attack
D	=	characteristic length of the projectile (diameter)
$F_{\cos}$, $F_{\sin}$	=	coefficient for the fast-mode contribution to the solution of state number
g	=	acceleration due to gravity
I_{XX}, I_{YY}, I_{ZZ}	=	moments of inertia of the projectile
$\tilde{L}$, $\tilde{M}$, $\tilde{N}$	=	external moments on a projectile expressed in the projectile body axes
m	=	mass of the projectile
$\tilde{p}$, $\tilde{q}$, $\tilde{r}$	=	components of the angular velocity vector of a projectile expressed in the no-roll reference frame
R_{MCM}, R_{MCP}	=	moment arm from the projectile center of gravity to the center of Magnus and center of pressure, respectively
$S_{\cos}$, $S_{\sin}$	=	coefficient for the slow-mode contribution to the solution of state number
s_i	=	nondimensional arc length of the ith range band
$\tilde{u}$, $\tilde{v}$, $\tilde{w}$	=	components of the translational velocity of the mass center of a projectile expressed in the no-roll reference frame.
$\tilde{u}_w$, $\tilde{v}_w$, $\tilde{w}_w$	=	components of the aerodynamic velocity of the mass center of a projectile expressed in the no-roll reference frame
V	=	velocity magnitude of the projectile
$\tilde{X}$, $\tilde{Y}$, $\tilde{Z}$	=	external forces on a projectile expressed in the projectile body axes
$\boldsymbol{X}_p$, $\boldsymbol{X}_\alpha$, $\boldsymbol{X}_e$	=	vectors containing the positional, rotational, and epicyclic states
$\boldsymbol{X}$	=	state vector of the projectile
$\boldsymbol{X}^I$, $\boldsymbol{X}^F$	=	state vector at launch condition and final impact point
x, y, z	=	components of the projectile position in the inertial reference frame
x_w, y_w, z_w	=	components of the atmospheric wind in the x, y, and z directions
$\boldsymbol{\Gamma}_i$	=	wind excitation vector for the ith arc-length segment
ζ_F, ζ_S	=	damping of the epicyclic fast and slow modes
ρ	=	local air density
σ_F, σ_S	=	real part of the epicyclic fast and slow modes
$\boldsymbol{\Phi}_i$	=	state-transition matrix for the ith arc-length segment

*Graduate Research Assistant, School of Aerospace Engineering. Student Member AIAA.
†Professor, School of Aerospace Engineering, School of Mechanical Engineering. Associate Fellow AIAA.
‡Associate Professor, Department of Mechanical and Aerospace Engineering. Senior Member AIAA.

ϕ, θ, ψ = Euler roll, pitch, and yaw angles of the projectile
ω_F, ω_S = imaginary part of the epicyclic fast and slow modes
$\omega_{n_F}, \omega_{n_S}$ = natural frequency of the epicyclic fast and slow modes
$()_0$ = initial condition of state number
$()'$ = derivative of state number with respect to arc length

Introduction

SEVERAL factors influence the accuracy of direct-fire projectiles, with one of the most important effects being atmospheric winds along the line of fire. Knowing the effect wind has on the flight path of a bullet and using that knowledge to make slight, precise aiming changes can mean the difference between hitting the intended target and missing completely. For long-range direct-fire shots, atmospheric winds are currently estimated through visual clues from the environment such as moving leaves, dust, or even mirage patterns seen in scopes. Detailed descriptions of these methods are found in the Army sniper training field manual [1]. These methods estimate the atmospheric winds at a single point along the projectile flight path, typically at the fire location. The relatively crude estimate of atmospheric wind speed and direction lead to a skewed estimate of the influence of atmospheric winds on the impact point of a fired projectile. This is particularly problematic for long-range shots through environments with complex atmospheric wind fields, including spatially varying wind structures. The advent of devices designed to measure atmospheric wind velocity in much finer detail such as small, rugged, and somewhat affordable laser-based light-detection and ranging systems, allow for detailed measurement and estimation of these winds. Systems such as these are capable of accurately estimating the three-dimensional wind velocity fields at a number of gates or ranges along the trajectory. To make use of this information, fire-control logic given a fire location, a final desired impact location, launch velocity, and spatially varying three-dimensional atmospheric wind velocity data, must compute the gun azimuth and elevation.

There currently exist fire-control methods based on nonlinear six-degree-of-freedom projectile models, relying on iterative numerical algorithms where the launch is simulated and the initial aim is adjusted based on the calculated impact-point error. These are relatively computationally expensive and time-consuming methods (see Bucco [2]). To improve computational efficiency, a table of fire-control solutions as a function of crosswind can be stored a priori and interpolated as needed. However, with complex measured atmospheric wind structures, it can be difficult to practically implement either of these approaches. For iterative methods, selecting an appropriate gun angle for the first iteration is difficult. Thus, a large and wide grid of various gun angles must be run to choose this starting point, further increasing the computational costs and time required to compute the fire-control solution. Breaux [3] recognized that methods using these six-degree-of-freedom models were not adequate when solution speed and efficiency was necessary and proposed using simplified models such as modified three-degree-of-freedom equation sets. While saving on computational cost, these methods based on simplified models sacrificed the final accuracy of the solution. For table interpolation methods, the dimensionality of the problem is greatly expanded.

A new computational algorithm for rapidly generating a fire-control solution for the case where spatially varying atmospheric wind velocity information is known precisely is proposed, one that is much faster than current fire-control methods while still maintaining a high level of accuracy. The algorithm uses a modified version of projectile linear theory with the key difference that measured wind profiles are estimated as ramp functions rather than step functions, as was documented by McCoy [4]. This modified projectile linear-theory model provides a solution in closed form, allowing it to be both accurately and rapidly computed. With this solution for the projectile's state, the fire-control problem can be solved analytically using a single noniterative numerical algorithm. It can also provide a solution more accurately than those based on more-restrictive equation sets such as a three-degree-of-freedom model. The particular linear-theory model used in the development of this algorithm is restricted to flat-fire trajectories but can easily be extended to trajectories with higher launch angles by using the linear-theory modifications suggested by Hainz and Costello [5]. The new algorithm is simple and well suited for field portable computers that can provide a shooter a rapid aiming solution. To motivate the need for this algorithm, the effect of atmospheric winds on the trajectory of a shot in each spatial dimension is examined and characterized. The proposed algorithm is applied to a direct-fire projectile for four classes of atmospheric wind velocity profiles and is shown to work well for all scenarios examined. The effects of wind-measurement resolution are investigated, such as the location and number of wind measurements. Finally, a Monte Carlo simulation is performed to show that using a resolved wind-estimation profile results in higher accuracy than single-point or even average atmospheric wind estimation. In all of the studies and simulations of this algorithm, it is assumed that the measurements of the wind velocities and directions are perfect.

Fire-Control Problem

Solving the fire-control problem amounts to aiming a gun so that a projectile hits a desired target. If the launch point, impact point, projectile exterior ballistics, and atmospheric conditions along the line of fire are all known, then the necessary gun elevation and azimuth to hit the target can be calculated. A part of the required input information is the atmospheric wind velocity field. An accurate model of the spatially varying wind can be crucial in accurately finding the correct solution and hitting the target. Figure 1 outlines this principle. The far left panel of the figure shows the true wind profile along the projectile line of fire, while the three rows to the right show how the accuracy of the shot can be affected based on how the estimate of the wind profile is obtained. In the first row, the wind is not considered at all, and so the zeroed scope is pointed directly at the target, but because there is in fact atmospheric wind, the launch results in a target miss. The second row shows what happens when the wind along the range is estimated by only considering the wind at the launch point, but again because true wind varies along the range and the wind is assumed constant, the result is a miss. Finally, the third row shows that measuring the atmospheric wind at multiple, discrete locations leads to an estimated wind profile that closely approximates the true profile. This more-accurate estimation leads to increased likelihood that a shot will hit the intended target.

A typical scenario for its use is as follows. First, the shot conditions such as the shooter location, target location, mass and aerodynamic properties of the projectile, and the initial projectile launch velocities are noted. Next, an atmospheric wind-measurement system is used to estimate the atmospheric wind profile between the shooter and the target. With this information known, the algorithm will use modified projectile linear theory to compute the necessary fire azimuth and elevation for successful target impact.

Projectile Dynamic Model

A six-degree of freedom rigid-body model is employed to predict the dynamics of a projectile in flight to validate the accuracy of the fire-control solution. The six degrees of freedom are composed of the three translational components describing the position of the projectile's center of mass as well as the three Euler angles describing the orientation of the projectile. Figures 2 and 3 provide a visualization of these six degrees of freedom. These equations of motion are well documented in the literature. See McCoy [4], Hainz and Costello [5], Costello and Peterson [6], and Frost and

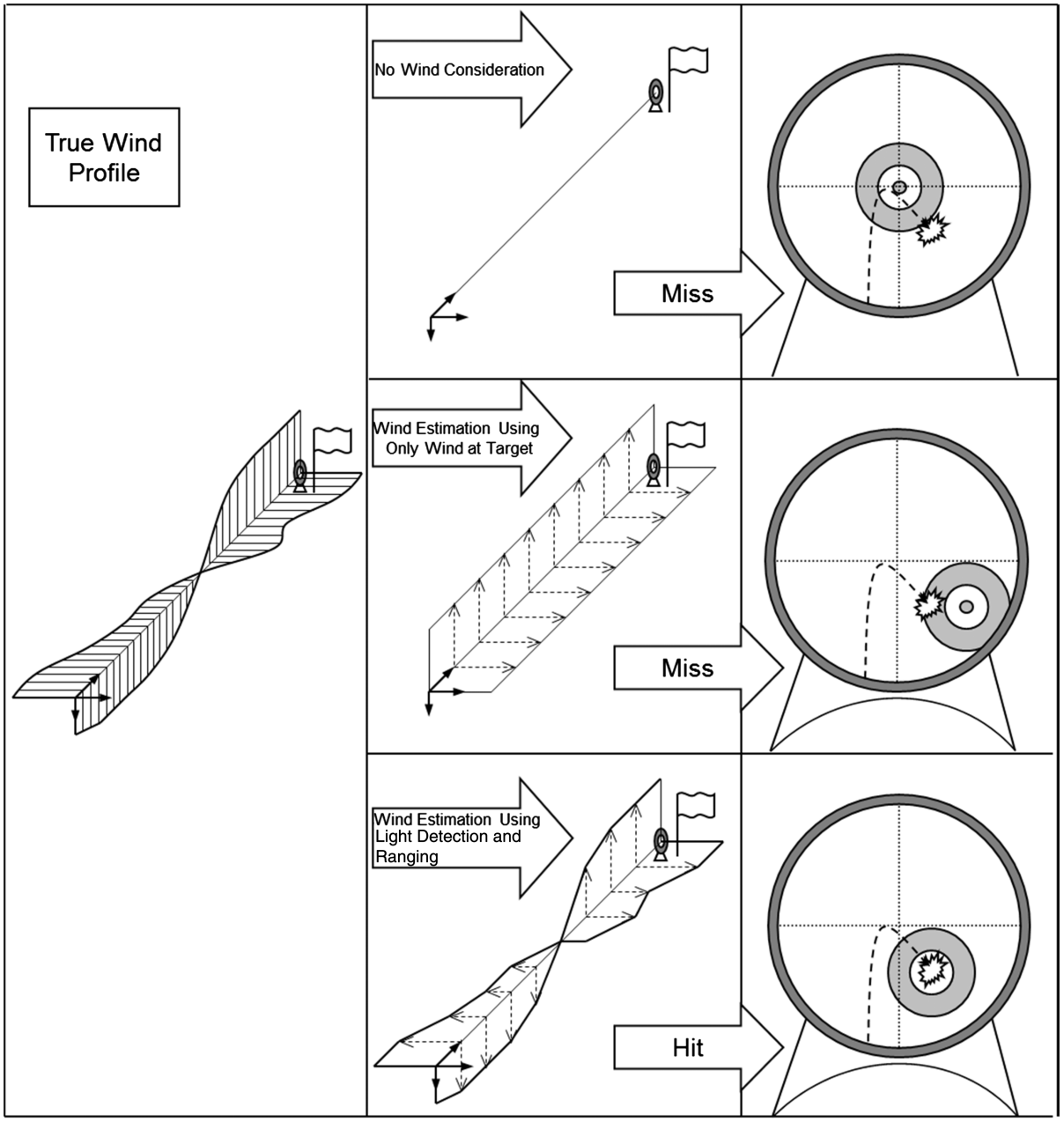

Fig. 1 Schematic showing the value of considering spatial winds in the fire-control solution.

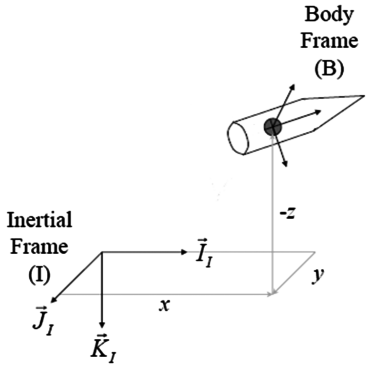

Fig. 2 Projectile position coordinate definitions.

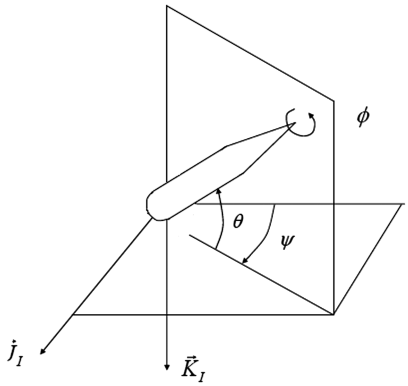

Fig. 3 Projectile orientation definitions.

Costello [7] for examples. The resulting 12 ordinary differential equations are highly nonlinear and do not lend themselves to a closed-form solution. These equations are typically solved numerically to generate a trajectory from known initial conditions.

Impact Error Due to Neglecting Spatially Varying Winds

The Army sniper training field manual [1] suggests a "clock system" for determining the effect of winds on a bullet's path. If the wind is coming from a headwind or tailwind direction, it is considered to have "no value" or very little effect on the projectile trajectory. When the wind is only coming from a crosswind direction it is considered to be at "full value" and has the greatest effect on the path of the projectile. The manual does not mention adjusting for the winds in the vertical direction. McCoy [8] also analytically investigated this phenomenon previously. An investigation was performed to both observe the effect that wind can have on the final impact point of a projectile and to quantitatively check the validity of the sniper training manual's recommendations. Toward this goal, a typical direct fire was simulated out to a range of 2000 m while varying the atmospheric winds from -10 to 10 m/s in each direction independently and calculating the radial error relative to the zero-wind impact point. Figure 4 shows the projectile impact drift due to winds varying in the x, y, and z directions. Based on these figures, it is noted that the effect of headwinds and tailwinds is three orders of magnitude less than the effects of crosswinds and vertical winds, supporting the idea that winds in the down range direction have no value and crosswinds have full value when considering adjustments for wind. However, it should also be noted that the vertical wind, in addition to the crosswind, has a significant influence on the impact point of a projectile. With this in mind, the proposed fire-control algorithm takes spatially varying winds in all three directions into account so that the resulting fire-control solutions will be more accurate.

Projectile Linear Theory for Spatially Varying Winds

Simplifications to the nonlinear rigid-body projectile flight dynamic equations have been identified over time, which yield an accurate, analytically solvable set of quasi-linear differential equations. The resulting equations are called projectile linear theory. McCoy [4] shows the development of projectile linear theory. Projectile linear theory provides more accurate trajectory predictions relative to other simplified models such as modified point mass and three-degree-of-freedom models as shown by Hainz and Costello [5]. To develop the projectile linear-theory equations, the following set of simplifications are employed. The station line velocity $\tilde{u}$, roll rate $\tilde{p}$, and roll angle ϕ are large in relation to the side velocities $\tilde{v}$ and $\tilde{w}$, yaw angle ψ, pitch and yaw rates $\tilde{q}$ and $\tilde{r}$, and wind velocity components $\tilde{u}_w$, $\tilde{v}_w$, and $\tilde{w}_w$. Products of small quantities and derivatives of small quantities are treated as negligible. The yaw angle ψ and aerodynamic angles of attack are assumed small in regard to trigonometric relations. The projectile is also assumed to be geometrically and aerodynamically symmetric about its axis. Projectile linear theory also introduces a change of variables in which the station line velocity $\tilde{u}$ is replaced by the projectile total velocity V. Another change of variables is employed to convert the independent variable time t to dimensionless arc length s, a dimensionless "time" measure that expresses the projectile's

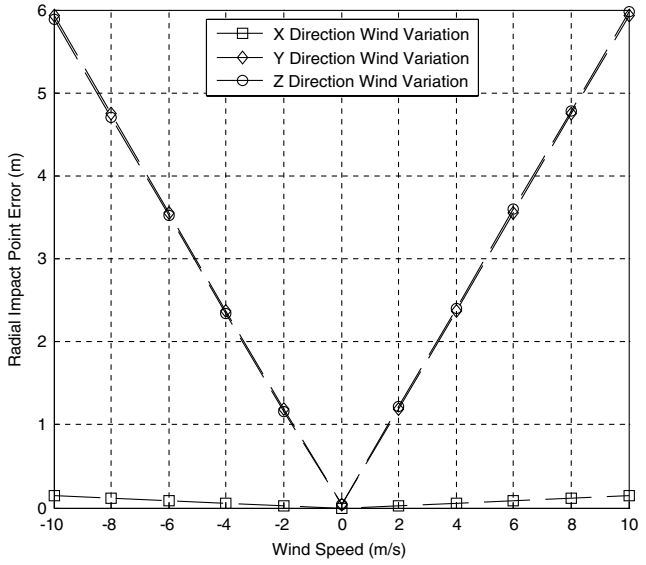

Fig. 4 Radial impact-point error of a projectile due to atmospheric winds in all spatial directions.

downrange travel in units of calibers. For equations in the arc-length domain, prime terms are used to denote arc-length derivatives, and dotted terms denote time derivatives. Applying these assumptions and transformations to the basic equations of motion yields the set shown in Eqs. (1–12):

$$x' = D \tag{1}$$

$$y' = D\psi + \frac{D}{V}\tilde{v} \tag{2}$$

$$z' = -D\theta + \frac{D}{V}\tilde{w} \tag{3}$$

$$\phi' = \frac{D}{V}\tilde{p} \tag{4}$$

$$\theta' = \frac{D}{V}\tilde{q} \tag{5}$$

$$\psi' = \frac{D}{V}\tilde{r} \tag{6}$$

$$V' = -\frac{\pi\rho D^3 C_{x0}}{8m}V - \frac{Dg}{V}s_\theta \tag{7}$$

$$\tilde{v}' = -\frac{\pi\rho D^3 C_{NA}}{8m}(\tilde{v} - \tilde{v}_w) - D\tilde{r} \tag{8}$$

$$\tilde{w}' = -\frac{\pi\rho D^3 C_{NA}}{8m}(\tilde{w} - \tilde{w}_w) + D\tilde{q} + \frac{Dgc_\theta}{V} \tag{9}$$

$$\tilde{p}' = \frac{\pi\rho V D^4 C_{LDD}}{8I_{XX}} + \frac{\pi\rho D^5 C_{LP}}{16I_{XX}}\tilde{p} \tag{10}$$

$$\tilde{q}' = \frac{\pi\rho D^4 R_{MCM} C_{YPA}}{16I_{YY}V}\tilde{p}(\tilde{v} - \tilde{v}_w) + \frac{\pi\rho D^3 R_{MCP} C_{NA}}{8I_{YY}}(\tilde{w} - \tilde{w}_w) + \frac{\pi\rho D^5 C_{MQ}}{16I_{YY}}\tilde{q} - \frac{I_{XX}D}{I_{YY}V}\tilde{p}\,\tilde{r} \tag{11}$$

$$\tilde{r}' = \frac{\pi\rho D^3 R_{MCP} C_{NA}}{8I_{YY}}(\tilde{v} - \tilde{v}_w) + \frac{\pi\rho D^4 R_{MCM} C_{YPA}}{16I_{YY}V}\tilde{p}(\tilde{w} - \tilde{w}_w) + \frac{I_{XX}D}{I_{YY}V}\tilde{p}\,\tilde{q} + \frac{\pi\rho D^5 C_{MQ}}{16I_{YY}}\tilde{r} \tag{12}$$

Although not strictly linear, these equations are in a form that makes an approximate analytical closed-form solution possible. This closed-form solution is obtained by holding the velocity and roll rate constant in all equations except for the equations for velocity and roll rate [Eqs. (7) and (10)]. This constant velocity and roll rate, along with and the atmospheric winds, are used to calculate all of the aerodynamic coefficients and solve the remaining equations. However, as the solution propagates downrange and velocity and roll rate change significantly, the closed-form solutions are updated with newly calculated velocity and roll rate values in desired arc-length intervals.

Previously, modified projectile linear theory presented by Hainz and Costello [5] and McCoy [4] treated the winds in each arc-length update segment as constants and only in the horizontal plane. For the fire-control algorithm reported here, projectile linear theory was modified such that atmospheric winds are treated as varying linearly between each arc-length update segments. Winds in the vertical direction are also included to account for all three spatial dimensions. To accommodate this extension, the projectile linear-theory equations are modified. In particular, atmospheric excitation terms appear as a ramp inputs to the system in lieu of the step function representation seen previously. This representation of the atmospheric winds for each direction is shown next over the ith arc-length band in Eqs. (13–17). Equations (16) and (17) are substituted into Eqs. (8–12):

$$x_w = m_x(s_{i+1} - s_i) + l_x \tag{13}$$

$$y_w = m_y(s_{i+1} - s_i) + l_y \tag{14}$$

$$z_w = m_z(s_{i+1} - s_i) + l_z \tag{15}$$

$$v_w = -\sin(\psi)x_w + \cos(\psi)y_w \tag{16}$$

$$w_w = \sin(\theta)\cos(\psi)x_w + \sin(\theta)\sin(\psi)y_w + \cos(\theta)z_w \tag{17}$$

In the previous equations, m_x, m_y, and m_z represent the slopes between the winds in the x, y, and z directions at each range gate, while l_x, l_y and l_z represent the wind in the x, y, and z directions at the start of each arc-length segment. Note that s is the arc-length value. Atmospheric wind values are obtained at discrete range locations using a wind-measurement system. For the purposes of this paper, these measurements are assumed to be perfect to highlight the algorithm. With these modifications for ramp winds, Eqs. (1–12) can be integrated in terms of dimensionless arc length as follows. Equations (8), (9), (11), and (12) form a coupled system of four linear differential equations that are solved, resulting in the epicyclic solution. The epicyclic solution is then integrated through Eqs. (5) and (6) to yield the orientation solution for the θ and ψ Euler angle solutions, which are then integrated again through Eqs. (2) and (3), yielding the y and z trajectory swerve solution. Equations (1), (7), and (10) are simple first-order linear differential equations that can be solved directly to give the range, velocity, and roll rate solutions. The roll rate solution can be integrated once to give the ϕ Euler angle solution. All of the solution equations for the projectile states are shown next in terms of nondimensional arc length, where the initial conditions are embedded linearly in the coefficients with a subscript of zero. The definitions of all the coefficients are included in the appendix.

$$x(s) = x_0 + Ds \tag{18}$$

$$y(s) = y_0 + C_{y_s}s + C_{y_{ss}}s^2 + C_{y_{sss}}s^3 + F_{y_{\cos}}e^{-\sigma_F s}\cos(\omega_F s) + F_{y_{\sin}}e^{-\sigma_F s}\sin(\omega_F s) + S_{y_{\cos}}e^{-\sigma_S s}\cos(\omega_S s) + S_{y_{\sin}}e^{-\sigma_S s}\sin(\omega_S s) \tag{19}$$

$$z(s) = z_0 + C_z s + C_{z_{ss}}s^2 + C_{z_{sss}}s^3 + F_{z_{\cos}}e^{-\sigma_F s}\cos(\omega_F s) + F_{z_{\sin}}e^{-\sigma_F s}\sin(\omega_F s) + S_{z_{\cos}}e^{-\sigma_S s}\cos(\omega_S s) + S_{z_{\sin}}e^{-\sigma_S s}\sin(\omega_S s) \tag{20}$$

$$\phi(s) = \phi_0 + C_{\phi s}s + C_{\phi e}e^{B_p s} \tag{21}$$

$$\theta(s) = \theta_0 + C_{\theta_s}s + C_{\theta_{ss}}s^2 + F_{\theta_{\cos}}e^{-\sigma_F s}\cos(\omega_F s) + F_{\theta_{\sin}}e^{-\sigma_F s}\sin(\omega_F s) + S_{\theta_{\cos}}e^{-\sigma_S s}\cos(\omega_S s) + S_{\theta_{\sin}}e^{-\sigma_S s}\sin(\omega_S s) \tag{22}$$

$$\psi(s) = \psi_0 + C_{\psi_s}s + C_{\psi_{ss}}s^2 + F_{\psi_{\cos}}e^{-\sigma_F s}\cos(\omega_F s) + F_{\psi_{\sin}}e^{-\sigma_F s}\sin(\omega_F s) + S_{\psi_{\cos}}e^{-\sigma_S s}\cos(\omega_S s) + S_{\psi_{\sin}}e^{-\sigma_S s}\sin(\omega_S s) \tag{23}$$

$$V(s) = \sqrt{\left(V_0^2 + \frac{B_V}{A_V}\right)e^{2A_V s} - \frac{B_V}{A_V}} \tag{24}$$

$$\tilde{v}(s) = \tilde{v}_0 + C_{v_s}s + F_{v_{\cos}}e^{-\sigma_F s}\cos(\omega_F s) + F_{v_{\sin}}e^{-\sigma_F s}\sin(\omega_F s) + S_{v_{\cos}}e^{-\sigma_S s}\cos(\omega_S s) + S_{v_{\sin}}e^{-\sigma_S s}\sin(\omega_S s) \tag{25}$$

$$\tilde{w}(s) = \tilde{w}_0 + C_{w_s}s + F_{w_{\cos}}e^{-\sigma_F s}\cos(\omega_F s) + F_{w_{\sin}}e^{-\sigma_F s}\sin(\omega_F s) + S_{w_{\cos}}e^{-\sigma_S s}\cos(\omega_S s) + S_{w_{\sin}}e^{-\sigma_S s}\sin(\omega_S s) \tag{26}$$

$$p(s) = -\frac{A_p}{B_p} + \left(P_0 + \frac{A_p}{B_p}\right)e^{B_p s} \tag{27}$$

$$\tilde{q}(s) = \tilde{q}_0 + C_{q_s}s + F_{q_{\cos}}e^{-\sigma_F s}\cos(\omega_F s) + F_{q_{\sin}}e^{-\sigma_F s}\sin(\omega_F s) + S_{q_{\cos}}e^{-\sigma_S s}\cos(\omega_S s) + S_{q_{\sin}}e^{-\sigma_S s}\sin(\omega_S s) \tag{28}$$

$$\tilde{r}(s) = \tilde{r}_0 + C_{r_s}s + F_{r_{\cos}}e^{-\sigma_F s}\cos(\omega_F s) + F_{r_{\sin}}e^{-\sigma_F s}\sin(\omega_F s) + S_{r_{\cos}}e^{-\sigma_S s}\cos(\omega_S s) + S_{r_{\sin}}e^{-\sigma_S s}\sin(\omega_S s) \tag{29}$$

Let the initial condition arc length be denoted as s_i and another arc length be s_{i+1}, then the previous solution can be written as

$$\begin{Bmatrix} y(s_{i+1}) \\ z(s_{i+1}) \\ \theta(s_{i+1}) \\ \psi(s_{i+1}) \\ \tilde{v}(s_{i+1}) \\ \tilde{w}(s_{i+1}) \\ \tilde{q}(s_{i+1}) \\ \tilde{r}(s_{i+1}) \end{Bmatrix} = [\Phi_i]\begin{Bmatrix} y(s_i) \\ z(s_i) \\ \theta(s_i) \\ \psi(s_i) \\ \tilde{v}(s_i) \\ \tilde{w}(s_i) \\ \tilde{q}(s_i) \\ \tilde{r}(s_i) \end{Bmatrix} + \{\Gamma_i\} \tag{30}$$

In shorthand,

$$\boldsymbol{X}(s_{i+1}) = \Phi_i \boldsymbol{X}(s_i) + \boldsymbol{\Gamma}_i \tag{31}$$

This equation can be applied recursively to construct a trajectory. Consider the solution at s_{i+3}:

$$\boldsymbol{X}(s_{i+3}) = \Phi_2\boldsymbol{X}(s_{i+2}) + \boldsymbol{\Gamma}_2 = \Phi_2(\Phi_1\boldsymbol{X}(s_{i+1}) + \boldsymbol{\Gamma}_1) + \boldsymbol{\Gamma}_2 = \Phi_2\Phi_1\boldsymbol{X}(s_{i+1}) + \Phi_2\boldsymbol{\Gamma}_1 + \boldsymbol{\Gamma}_2 = \Phi_2\Phi_1(\Phi_0\boldsymbol{X}(s_i) + \boldsymbol{\Gamma}_0) + \Phi_2\boldsymbol{\Gamma}_1 + \boldsymbol{\Gamma}_2$$
$$= [\Phi_2\Phi_1\Phi_0]\boldsymbol{X}(s_i) + (\Phi_2\Phi_1\boldsymbol{\Gamma}_0 + \Phi_2\boldsymbol{\Gamma}_1 + \boldsymbol{\Gamma}_2) \tag{32}$$

In general,

$$\boldsymbol{X}(s_{i+n}) = M\boldsymbol{X}(s_i) + \boldsymbol{B} \quad \text{where } M = \prod_{k=0}^{n-1}\Phi_k \quad \boldsymbol{B} = \sum_{k=0}^{n-2}\left(\left(\prod_{l=k+1}^{n-1}\Phi_l\right)\boldsymbol{\Gamma}_k + \boldsymbol{\Gamma}_{n-1}\right) \tag{33}$$

It should be noted that the vector $\boldsymbol{\Gamma}_i$ contains forcing function terms in the ith arc-length band such as atmospheric winds.

Fire-Control Solution

The fire-control problem is a two-point boundary-value problem with the following known and unknown states. The initial fire location coordinates x_i, y_i, z_i are known values as are the initial muzzle velocity V_i and spin rate p_i. With no loss in generality, the initial roll angle ϕ is assumed to be zero. The initial epicyclic states $\tilde{v}_i$, $\tilde{w}_i$, $\tilde{q}_i$, and $\tilde{r}_i$ are also assumed to be zero, although if values for these states are known at launch, they can be easily implemented into the algorithm development. The last remaining initial states are the gun-pointing angles θ_i and ψ_i, which are ultimately what is to be calculated. The only final states known are the desired impact-point coordinates x_F, y_F, z_F.

The projectile linear-theory equations are such that the velocity, roll rate, range, and roll angle equations V, x, p, and ϕ are uncoupled from the remaining states. Because the initial conditions are known for all four of these uncoupled states, each can be computed across the entire trajectory independent of the remaining states.

For ease of bookkeeping, the eight states remaining are placed into three groups as shown in Eq. (34):

$$\boldsymbol{X} = [\,\boldsymbol{X}_p \quad \boldsymbol{X}_\alpha \quad \boldsymbol{X}_e\,]^T \tag{34}$$

where $\boldsymbol{X}_p = [\,y \quad z\,]^T$ contains position states, $\boldsymbol{X}_\alpha = [\,\theta \quad \psi\,]^T$ contains orientation states, and $\boldsymbol{X}_e = [\,\tilde{v} \quad \tilde{w} \quad \tilde{q} \quad \tilde{r}\,]^T$ contains epicyclic states. Let s_{i+n} represent the impact point or $\boldsymbol{X}(s_{i+n}) = \boldsymbol{X}^F$, and let s_i represent the launch conditions or $\boldsymbol{X}(s_i) = X^I$. Using the solution form given by Eq. (33) and the previous state partition,

$$\begin{Bmatrix} \boldsymbol{X}_P^F \\ \boldsymbol{X}_\alpha^F \\ \boldsymbol{X}_e^F \end{Bmatrix} = \begin{bmatrix} M_{11} & M_{12} & M_{13} \\ M_{21} & M_{22} & M_{23} \\ M_{31} & M_{32} & M_{33} \end{bmatrix} \begin{Bmatrix} \boldsymbol{X}_P^I \\ \boldsymbol{X}_\alpha^I \\ \boldsymbol{X}_e^I \end{Bmatrix} + \begin{Bmatrix} B_1 \\ B_2 \\ B_3 \end{Bmatrix} \tag{35}$$

This reduces the problem to a system of algebraic equations. Because the only states of interest to the fire-control solution are the initial Euler angles (θ_i, ψ_i), only one row of this block system needs to be solved. The first row of Eq. (35) can be expanded and solved for the initial orientation state. This is shown in Eq. (36), the solution to which gives the closed-form fire-control solution. The other two rows of the system shown in Eq. (35) can then be solved to find the final orientation and epicyclic states, but because this does not help with the fire-control problem, these computations need not be performed:

$$\boldsymbol{X}_\alpha^I = \begin{Bmatrix} \theta^I \\ \psi^I \end{Bmatrix} = M_{12}^{-1}(\boldsymbol{X}_p^F - M_{11}\boldsymbol{X}_p^I - M_{13}\boldsymbol{X}_e^I - \mathbf{B}_1) \tag{36}$$

Practical implementation of the fire-control algorithm begins by noting the initial projectile position (x_i, y_i, z_i or $\boldsymbol{X}_p^I$), intended target position (x_F, y_F, z_F or $\boldsymbol{X}_p^F$), initial velocity V_i, initial roll rate p_i, air density, speed of sound, projectile mass properties, projectile aerodynamic coefficient

Table 1 Aerodynamic data for projectile used

Mach number	CXO	CX2	CNA	CLDD	CLP	CMA	CMQ
1.00E + 00	1.04E + 00	1.16E + 01	2.12E + 01	7.65E − 02	−2.49E + 01	−205.2	−8.18E + 03
1.03E + 00	1.13E + 00	1.25E + 01	2.13E + 01	7.70E − 02	−2.52E + 01	−209	−8.27E + 03
1.05E + 00	1.22E + 00	1.35E + 01	2.15E + 01	7.80E − 02	−2.54E + 01	−212.9	−8.37E + 03
1.10E + 00	1.42E + 00	1.54E + 01	2.19E + 01	7.95E − 02	−2.59E + 01	−219.1	−8.60E + 03
1.20E + 00	1.38E + 00	1.86E + 01	2.20E + 01	7.95E − 02	−2.60E + 01	−219.8	−8.68E + 03
1.35E + 00	1.37E + 00	1.80E + 01	2.17E + 01	7.85E − 02	−2.56E + 01	−215.6	−8.67E + 03
1.50E + 00	1.33E + 00	1.75E + 01	2.11E + 01	7.65E − 02	−2.50E + 01	−205.8	−8.53E + 03
1.75E + 00	1.25E + 00	1.69E + 01	2.08E + 01	7.65E − 02	−2.49E + 01	−198.7	−8.43E + 03
2.00E + 00	1.18E + 00	1.63E + 01	2.00E + 01	7.25E − 02	−2.36E + 01	−194.8	−8.00E + 03
2.25E + 00	1.11E + 00	1.60E + 01	1.94E + 01	7.05E − 02	−2.30E + 01	−178.4	−7.76E + 03
2.50E + 00	1.04E + 00	1.57E + 01	1.88E + 01	6.85E − 02	−2.23E + 01	−162.1	−7.52E + 03
3.00E + 00	9.05E − 01	1.39E + 01	1.76E + 01	6.20E − 02	−2.02E + 01	−131.6	−7.05E + 03
3.50E + 00	7.97E − 01	1.30E + 01	1.65E + 01	5.55E − 02	−1.82E + 01	−113.4	−6.57E + 03
4.00E + 00	6.90E − 01	1.22E + 01	1.54E + 01	4.95E − 02	−1.61E + 01	−95.2	−6.09E + 03
4.50E + 00	6.16E − 01	1.13E + 01	1.43E + 01	4.50E − 02	−1.48E + 01	−84.7	−5.61E + 03
5.00E + 00	5.43E − 01	1.04E + 01	1.32E + 01	4.10E − 02	−1.34E + 01	−74.2	−5.13E + 03
6.00E + 00	4.80E − 01	9.44E + 00	1.09E + 01	3.65E − 02	−1.20E + 01	−61.3	−4.60E + 03
8.00E + 00	4.49E − 01	9.08E + 00	9.92E + 00	3.55E − 02	−1.14E + 01	−55.8	−4.22E + 03

CXO, Axial Force Coefficient; CX2, Axial Force Coefficient with Respect to Angle of Attack Squared; CAN, Normal Force Coeffcient; CLDD, Roll Moment Coefficient Due to Fin Cant; CLP, Roll Damping Coefficient; CMA, Pitch Moment Coefficient; CMQ, Pitch Damping Coefficient.

tables, arc-length update interval, and measured atmospheric wind data. With all of the input data available, the main loop through the arc-length update intervals begins to construct the entries in Eq. (33). The algorithm first calculates the velocity and roll rate at the current arc-length interval along with the corresponding aerodynamic coefficients. Then, through interpolation of the spatial atmospheric winds data, the ramp function for wind over the arc-length interval is generated. The state-transition matrix and forcing vector are then computed. See Ollerenshaw and Costello [9] for more details on an efficient method to compute these matrices. After these state-transition matrices have been computed, they are combined with the matrices from the previous arc-length update intervals. With the values for Eqs. (35) and (36) now available, the fire-control solution is computed and output.

Results

To exercise the algorithm detailed previously, it is applied to an example finned projectile in a direct-fire mission operating in a spatially varying atmospheric wind field. To generate results and validate the accuracy of the fire-control solution, simulated trajectory data are generated with an industry standard, rigid-body, six-degree-of-freedom model that is fully nonlinear called BOOM [10]. The example projectile used was a standard fin-stabilized projectile with a weight of 50 N and a reference diameter of 0.027 m. The mass center is located on the axis of rotation and is 0.42 m from the base of the round. The inertia matrix is diagonal with elements of 0.0003236, 0.24, and 0.24 $\text{kg} \cdot \text{m}^2$. Aerodynamic data for the projectile can be found in Table 1. For all cases considered, the projectile is fired with a velocity of 850 m/s and a spin rate of 8.7 rad/s. All measured winds considered are assumed to be precisely known.

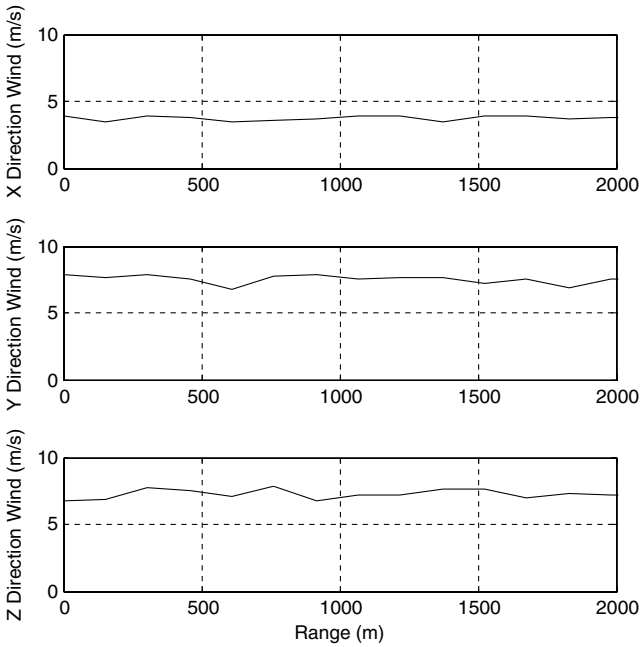

Fig. 5 Atmospheric wind field used in the constant wind case study.

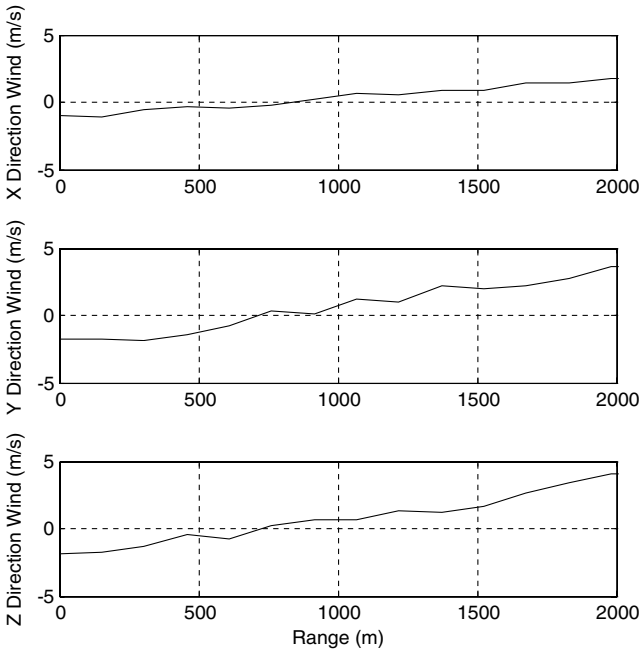

Fig. 6 Atmospheric wind field used in the linearly varying wind profile.

An example projectile is simulated to a range of 2 km from the shooter. The launch position, muzzle velocity, launch roll rate, intended impact point, projectile data, and sampled atmospheric wind data are used as input data by the fire-control algorithm. The proposed fire-control algorithm then computes the required gun azimuth and elevation. This azimuth and elevation is subsequently used as input to the fully nonlinear projectile flight simulation tool BOOM to calculate the trajectory of the projectile to the target along with the impact point. Because the intended impact point is prescribed, the actual impact point error can be computed. For all of the results to follow, this sequence of operations has been used to generate examples to explore the performance of the proposed algorithm.

To examine the speed and accuracy of the proposed algorithm, the algorithm was employed for four different types of wind fields with the goal, as stated, to strike a target in the y-z plane located 2000 m downrange. Figure 5 presents the first wind field type examined. It is simply constant valued atmospheric winds over the range of the shot with a small amount of noise superimposed on the constant value (standard deviation of 0.2 m at 16 points down range). Figure 6 shows the second type, which is a wind field that changes linearly over the range of the shot also containing a small amount of random noise. Figure 7 shows the third type of wind function tested. This wind is a nonlinearly varying wind that always points in the positive sense of each spatial direction as defined by the inertial reference axis used in the development of the previous projectile models. Figure 8 shows the last type of wind function used where the wind varies nonlinearly once again, but with the wind switching directions at some points along the range. After the proposed algorithm was used to compute an initial fire-angle solution, this solution is implemented into the rigid-body projectile simulation tool to test the fire-control solution accuracy. For all four atmospheric wind conditions, the terminal radial error was found to be less than 15 mm, validating this fire-control solution approach. It should be noted that, when time was nondimensionalized by the duration of the fire-control solution calculation, simulating a projectile trajectory took about 10 to 20 times longer to compute. Because the

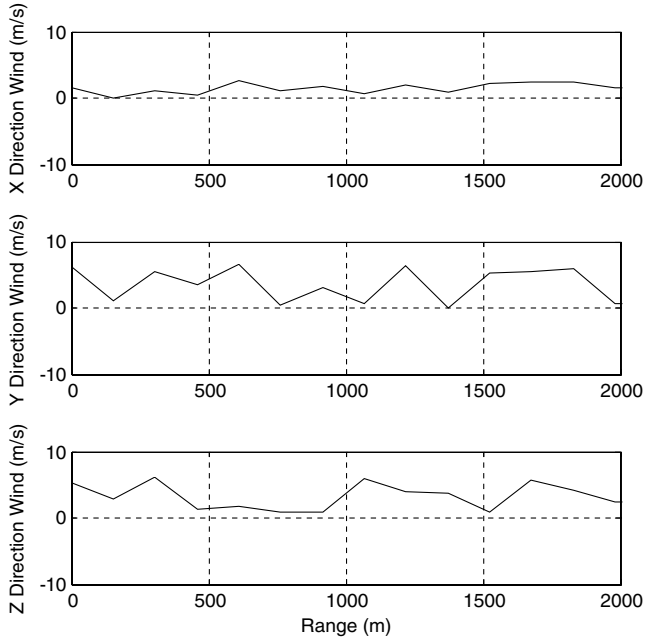

Fig. 7 Atmospheric wind field used in the positive-only nonlinearly varying case study.

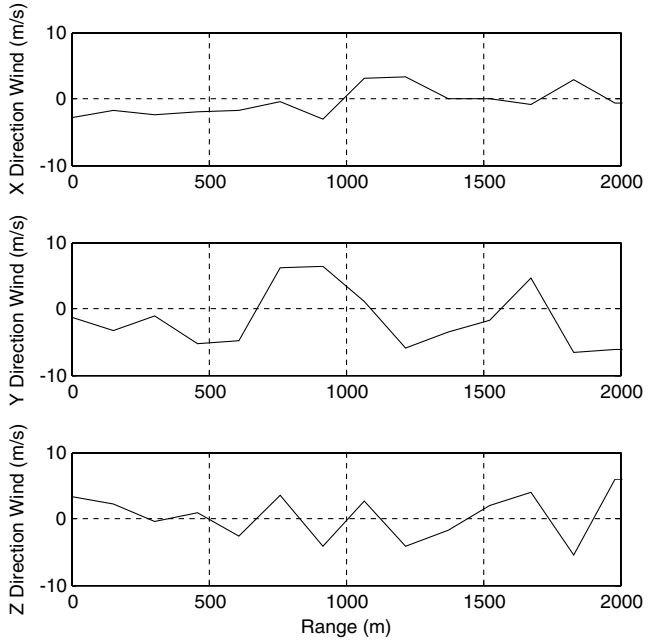

Fig. 8 Atmospheric wind field used in the positive–negative nonlinearly varying case study.

Table 2 Wind statistics and impact error for case studies

Wind type	Average x direction wind, m/s	Average y direction wind, m/s	Average z direction wind, m/s	Standard deviation x direction wind, m/s	Standard deviation y direction wind, m/s	Standard deviation z direction wind, m/s	Impact error, mm	Computation time, normalized computing unit
Constant	3.724	7.445	7.269	0.211	0.374	0.357	4.9	1.00
Linear	0.311	0.603	0.646	1.064	2.075	2.089	11.1	1.03
Positive nonlinear	1.433	3.434	3.190	0.821	2.452	1.865	7.4	1.08
Positive/negative nonlinear	−0.602	−1.379	0.742	2.068	4.503	3.458	16.2	1.07

simulation of the projectile trajectory uses numerical methods similar to current fire-control methods based on iterative routines, the new proposed method provides a large increase in solution speed and computing efficiency. A summary of wind field statistics, computation times and impact errors based on the fire-control solution for each of the four types of wind fields examined is shown in Table 2.

To illustrate the accuracy improvements possible with the proposed fire-control algorithm, a Monte Carlo simulation was used to generate impact-point error statistics for four difference wind-estimation scenarios. The first scenario considers a situation where all atmospheric wind conditions are measured along the trajectory and used in the subsequent fire-control solution (proposed algorithm). The second scenario considers a situation where atmospheric winds are measured near the gun muzzle and ignores the additional wind changes down range. It is assumed that the atmospheric winds are constant and equal to those measured at the muzzle. The third scenario is the same as the second scenario except the atmospheric wind measurement is made near the target. The fourth scenario measures an average of each directional component of the atmospheric wind field along the trajectory. Each Monte Carlo simulation uses 200 samples. These calculations are generated for two different wind fields. The first wind field is similar to a constant wind field (Figs. 5 and 6), while the second wind field resembles a nonlinear wind field (Figs. 7 and 8). The impact errors for each sample within the Monte Carlo simulation were counted and plotted as histograms for each wind-estimation scenario along with the average impact error for the 200 samples. Figure 9 shows this plot for the linear winds simulation, and Fig. 10 shows this plot for the nonlinear winds simulation. It can be seen that there is improved accuracy using the new fire-control method when the wind profile is mostly constant and linear winds, but the proposed algorithm truly excels in accuracy in cases where the measured wind is nonlinearly varying. In these atmospheric conditions, the algorithm provides significantly more-accurate and precise results than other methods described previously. The statistics for the wind used in this summary are very similar to those given in Table 2 for the corresponding wind profile.

The previous studies assumed that the atmospheric wind field is known continuously along the trajectory. This is not the case in a practical situation because the wind-detection systems are only capable of measuring the wind speeds at discrete points in space that are referred to as range gates. An important aspect relative to practical implementation is the number of discrete atmospheric wind measurements needed to achieve a particular fire-control solution accuracy. To investigate this issue, the four wind fields employed previously (Figs. 5–8) were sampled at different numbers of points along the trajectory where the measurement at each location is assumed to be perfect. For the purpose of the fire-control solution, the measured atmospheric wind values are interpolated as needed. An example of a varying number of sampled wind measurements versus the true wind field is shown in Fig. 11. Figure 12 presents statistical results showing the average impact-point error as a function of the number of equally spaced atmospheric wind measurements. The four previous different wind profiles are all considered (Figs. 5–8). The average

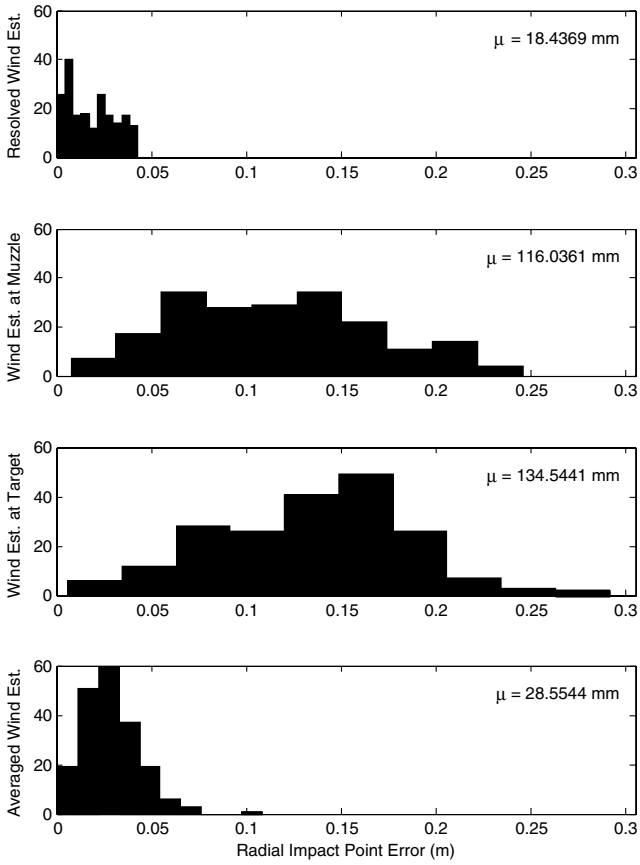

Fig. 9 Monte Carlo simulation histogram for impact error due to constant and linear wind fields.

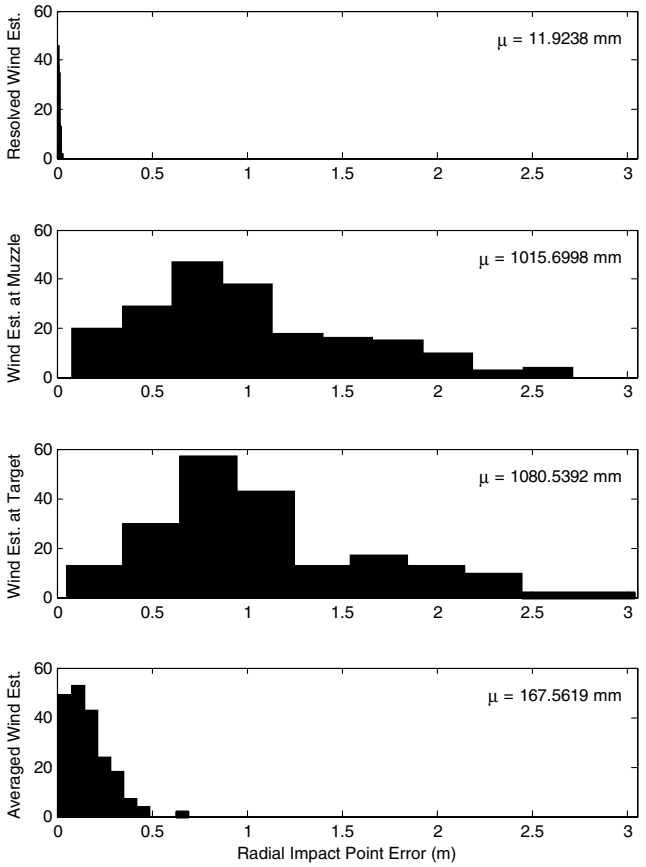

Fig. 10 Monte Carlo simulation histogram for impact error due to nonlinearly varying wind fields.

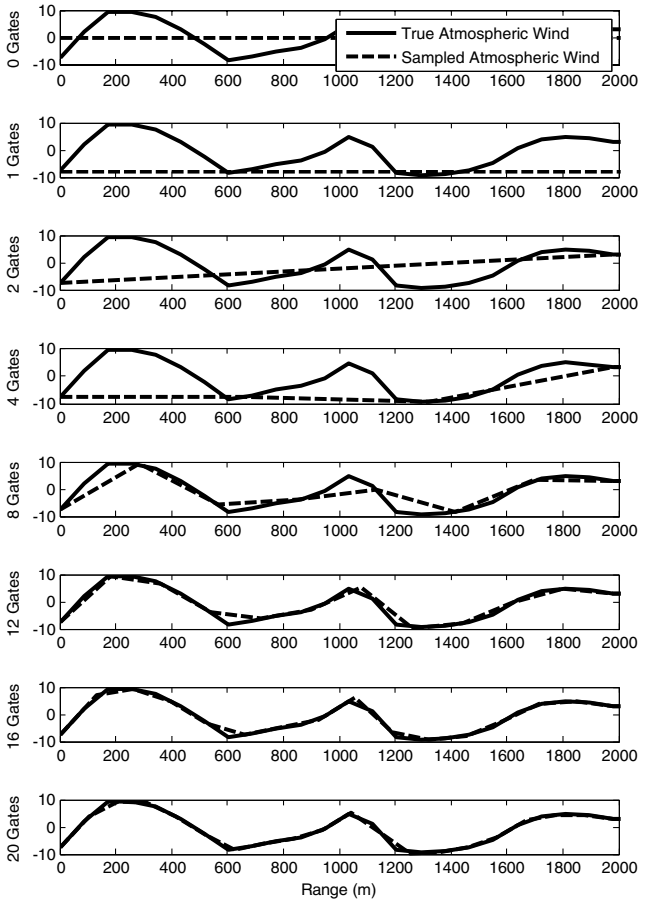

Fig. 11 Example of atmospheric wind field sampling used in the minimum number of range gates trade study.

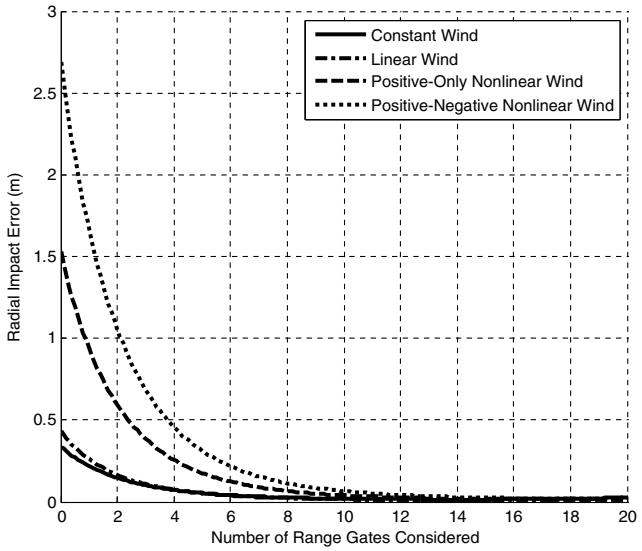

Fig. 12 Impact error vs number of range gates for the four wind functions used previously (see Figs. 5–8).

impact error is based on a sample size of 25. Figure 12 shows that, for all types of wind considered, the impact error decreases exponentially as the number of range gates considered increases. For the first two wind types, the constant and linearly varying winds, the impact error started high and decreased to a very small number with only 2–4 range gates, but increasing the number of gates beyond this number for wind fields of this type provides very little benefit compared to only using 2–4 measure locations. However, the second two wind types, both varying nonlinearly, showed that the decrease in error as the range gate number increased was much slower than for the first two wind forms. The error once again was seen to hit a point of diminishing returns after about 12 range gates for these winds. Thus, in ranges where the wind is seen to change nonlinearly down range, more range gate measurements are needed to computing an accurate solution than for steadier, more linearly behaving atmospheric winds. A statistical summary of the wind fields used in this study is given in Table 2.

A second important aspect relative to practical implementation is the distance from the target where atmospheric wind measurements can be obtained. This practical consideration stems from the fact that a wind velocity system that is gun mounted will have a certain maximum measurement range. A schematic of this scenario is shown in Fig. 13. Toward this end, Fig. 14 considers fire-control solution impact-point accuracy as a function of the maximum range of the atmospheric wind velocity measurement system. For the purpose of the fire-control solution, the atmospheric wind velocity beyond the measurement range is assumed to be equal to 0 or to the average of all measurements of a particular

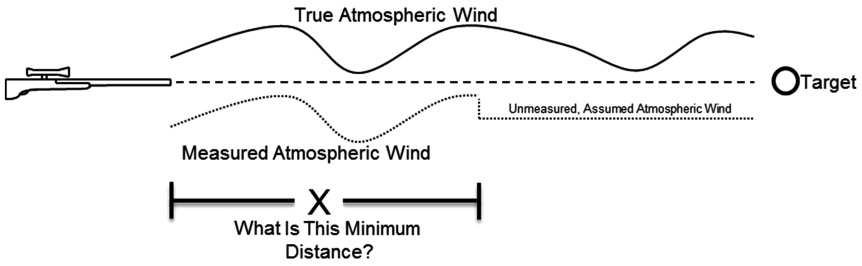

Fig. 13 Schematic of the motivation for the minimum measurement range trade study.

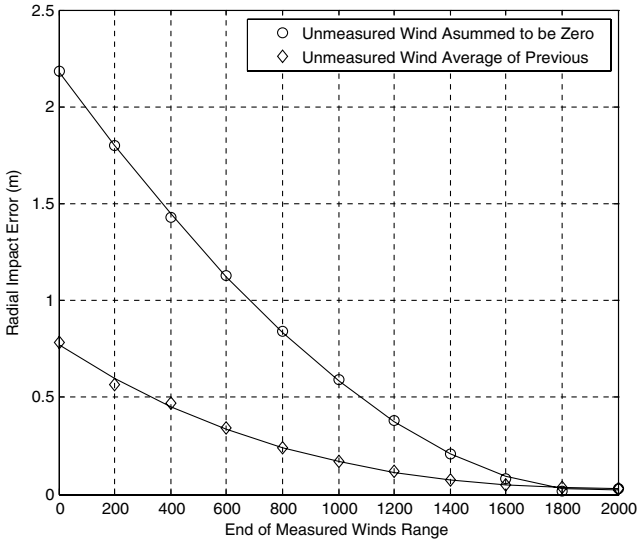

Fig. 14 Impact error vs range of final wind-speed measurement.

component. Figure 14 was generated with the same process as Fig. 12 but using only the positive-only nonlinearly varying. The results show a slow exponential decrease in impact error until the range of measurement is almost to the target range. It is also apparent that assuming the unmeasured winds downrange to be the average of the previous is much more accurate than assuming it to be zero, indicating that, if full-range measurement is not possible, the wind must be measured as far as possible toward the target, and the rest must be estimated to be the average of the measured wind for maximum accuracy.

Conclusions

A new fire-control algorithm was created that incorporates spatially varying winds into the fire-control solution. The new algorithm is based on an extended form of projectile linear theory, which enables a closed-form solution for the fire-control solution to be generated rapidly. To motivate the use of the algorithm, it is first shown that knowledge of cross winds and vertical winds are both important factors for the fire-control solution. The algorithm is shown to generate an accurate fire-control solution for varied atmospheric wind conditions, including cases with constant winds, linearly varying winds, and positive-only and positive–negative nonlinearly varying winds where all of the values are assumed to be perfectly accurate measurements of both direction and velocities of the wind. Each of these fire-control solutions is generated approximately 10–15 times faster than it takes to simulate the trajectory. Through the use of Monte Carlo simulation, it was shown that spatial atmospheric wind information allows significantly improved fire-control solutions, especially for nonlinearly varying wind fields. Ultimately, it was seen that the proposed algorithm indeed provided an accurate solution by considering more resolved atmospheric wind estimations and very rapidly by basing the algorithm on modified projectile linear theory. The algorithm should prove useful to weapon-system designers creating new fire-control solutions as more detailed atmospheric wind velocity information becomes available on new sensor systems.

Appendix Coefficients for Eqs. (18–29)

For a single arc-length step (subscript 0 denotes state at beginning of step); general aerodynamic coefficient definitions:

$$A = \frac{\pi\rho D^3 C_{NA}}{8m} \quad B = \frac{P_0(\pi\rho D^5 C_{YPA})(R_{MCM})}{16V_0 I_{yy}} \quad C = \frac{(\pi\rho D^4 C_{NA})(R_{MCP})}{8I_{yy}} \quad H = \frac{\pi\rho D^5 C_{MQ}}{16I_{yy}} \quad F = \frac{P_0 I_{xx} D}{V_0 I_{yy}}$$

Velocity, roll rate, and gravity coefficient definitions:

$$A_V = -\frac{\pi\rho D^3 C_{X0}}{8m} \quad B_V = -gD\,\sin(\theta) \quad A_P = \frac{\pi\rho V_0 D^4 C_{LDD}}{8I_{xx}} \quad B_P = \frac{\pi\rho D^5 C_{LP}}{16I_{xx}} \quad G = \frac{Dg\,\cos(\theta)}{V_0}$$

Spatial wind coefficient definitions:

$$\alpha = -\sin(\psi)l_x + \cos(\psi)l_y \quad \beta = -\sin(\psi)m_x + \cos(\psi)m_y \quad \gamma = \sin(\theta)\cos(\psi)l_x + \sin(\theta)\sin(\psi)l_y + \cos(\theta)l_z$$
$$\delta = \sin(\theta)\cos(\psi)m_x + \sin(\theta)\sin(\psi)m_y + \cos(\theta)m_z$$

Epicyclic eigenvalue calculation:

$$E_r = A^2 + 4C - F^2 + 2AH + H^2 \quad E_i = 2AF + 4B + 2FH \quad \varepsilon = a\,\tan 2(E_i, E_r) \quad E_{\text{tot}} = E_i^2 + E_r^2 \quad \sigma_F = \frac{1}{2}\left(H - A - \sqrt[4]{E_{\text{tot}}}\cos\left(\frac{\varepsilon}{2}\right)\right)$$
$$\omega_F = \frac{1}{2}\left(F - \sqrt[4]{E_{\text{tot}}}\sin\left(\frac{\varepsilon}{2}\right)\right) \quad \sigma_S = \frac{1}{2}\left(H - A + \sqrt[4]{E_{\text{tot}}}\cos\left(\frac{\varepsilon}{2}\right)\right) \quad \omega_S = \frac{1}{2}\left(F + \sqrt[4]{E_{\text{tot}}}\sin\left(\frac{\varepsilon}{2}\right)\right)$$

Natural frequency and damping ratio computation:

$$\omega_{n_F} = \sqrt{\sigma_F^2 + \omega_F^2} \quad \zeta_F = -\frac{\sigma_F}{\omega_{n_F}} \quad \omega_{n_S} = \sqrt{\sigma_S^2 + \omega_S^2} \quad \zeta_S = -\frac{\sigma_S}{\omega_{n_S}}$$

Coefficient inversion matrix:

$$\det = -\omega_{n_F}^4 + 2\omega_{n_F}^2\omega_{n_S}^2 - \omega_{n_S}^4 - 4\omega_{n_F}^2\omega_{n_S}^2\zeta_F^2 + 4\omega_{n_F}^3\omega_{n_S}\zeta_F\zeta_S + 4\omega_{n_F}\omega_{n_S}^3\zeta_F\zeta_S - 4\omega_{n_F}^2\omega_{n_S}^2\zeta_S^2$$

$$[\text{CIM}] = \frac{1}{\det}\begin{bmatrix} \omega_{n_F}^2 - \omega_{n_S}^2 - 4\omega_{n_F}^2\zeta_F^2 + 4\omega_{n_F}\omega_{n_S}\zeta_F\zeta_S & 2\omega_{n_F}^3\zeta_F - 2\omega_{n_F}^2\omega_{n_S}\zeta_S & -\omega_{n_F}^4 + \omega_{n_F}^2\omega_{n_S}^2 & 2\omega_{n_F}^3\omega_{n_S}^2\zeta_F + 2\omega_{n_F}^4\omega_{n_S}\zeta_S \\ -\omega_{n_F}^2 + \omega_{n_S}^2 + 4\omega_{n_F}\omega_{n_S}\zeta_F\zeta_s - 4\omega_{n_S}^2\zeta_S^2 & -2\omega_{n_F}\omega_{n_S}^2\zeta_F + 2\omega_{n_S}^3\zeta_S & \omega_{n_F}^2\omega_{n_S}^2 - \omega_{n_S}^4 & 2\omega_{n_F}\omega_{n_S}^4\zeta_F - 2\omega_{n_F}^2\omega_{n_S}^3\zeta_S \\ -2\omega_{n_F}\zeta_F + 2\omega_{n_S}\zeta_S & \omega_{n_F}^2 - \omega_{n_S}^2 & 2\omega_{n_F}\omega_{n_S}^2\zeta_F - 2\omega_{n_F}^2\omega_{n_S}\zeta_S & \omega_{n_F}^4 + \omega_{n_F}^2\omega_{n_S}^2 - 4\omega_{n_F}^2\omega_{n_S}^2\zeta_F^2 + 4\omega_{n_F}^3\omega_{n_S}\zeta_F\zeta_S \\ 2\omega_{n_F}\zeta_F - 2\omega_{n_S}\zeta_S & -\omega_{n_F}^2 + \omega_{n_S}^2 & -2\omega_{n_F}\omega_{n_S}^2\zeta_F + 2\omega_{n_F}^2\omega_{n_S}\zeta_S & \omega_{n_F}^2\omega_{n_S}^2 - \omega_{n_S}^4 + 4\omega_{n_F}\omega_{n_S}^3\zeta_F\zeta_S - 4\omega_{n_F}^2\omega_{n_S}^2\zeta_S^2 \end{bmatrix}$$

No-roll frame body y velocity coefficients:

$$
\begin{aligned}
N_{v0} &= B^2\beta + \beta C^2 + 2AB\beta F + A^2\beta F^2 + 2A\beta CH + A^2\beta H^2 \\
N_{v1} &= \alpha B^2 - 2A\beta C + \alpha C^2 + 2A\alpha BF + B\beta F + C\delta F + A^2\alpha F^2 + A\beta F^2 \\
&\quad - CFG - 2A^2\beta H + 2A\alpha CH + \beta CH - B\delta H + BGH + A^2\alpha H^2 + A\beta H^2 \\
N_{v2} &= A^2\beta - 2A\alpha C - \beta C + B\delta + \alpha BF + A\alpha F^2 - BG + CF\gamma - 2A^2\alpha H - 2A\beta H + \alpha CH - B\gamma H + A\alpha H^2 - BD\tilde{q}_0 - ADF\tilde{q}_0 \\
&\quad + CD\tilde{r}_0 + ADH\tilde{r}_0 + BF\tilde{v}_0 + AF^2\tilde{v}_0 + CH\tilde{v}_0 + AH^2\tilde{v}_0 - CF\tilde{w}_0 + BH\tilde{w}_0 + A\alpha F^2 - BG + CF\gamma - 2A^2\alpha H - 2A\beta H \\
&\quad + \alpha CH - B\gamma H + A\alpha H^2 - BD\tilde{q}_0 - ADF\tilde{q}_0 + CD\tilde{r}_0 + ADH\tilde{r}_0 + BF\tilde{v}_0 + AF^2\tilde{v}_0 + CH\tilde{v}_0 + AH^2\tilde{v}_0 - CF\tilde{w}_0 + BH\tilde{w}_0 \\
N_{v3} &= A^2\alpha + A\beta - \alpha C + B\gamma - 2A\alpha H - DF\tilde{q}_0 - AD\tilde{r}_0 + DH\tilde{r}_0 - C\tilde{v}_0 + F^2\tilde{v}_0 - 2AH\tilde{v}_0 + H^2\tilde{v}_0 - B\tilde{w}_0 \\
N_{v4} &= A\alpha - D\tilde{r}_0 + A\tilde{v}_0 - 2H\tilde{v}_0 \\
N_{v5} &= \tilde{v}_0 \\
C_{v_S} &= \frac{N_{v0}}{\omega_{n_F}^2\omega_{n_S}^2} \\
C_{v_0} &= \frac{N_{v1} - C_{v_S}(2\omega_{n_S}\zeta_S\omega_{n_F}^2 + 2\omega_{n_F}\zeta_F\omega_{n_S}^2)}{\omega_{n_F}^2\omega_{n_S}^2} \\
B_{v1} &= N_{v2} - C_{v_0}(2\zeta_F\omega_{n_F}\omega_{n_S}^2 + 2\zeta_S\omega_{n_S}\omega_{n_F}^2) - C_{v_S}(\omega_{n_S}^2 + \omega_{n_F}^2 + 4\omega_{n_F}\omega_{n_S}\zeta_F\zeta_S) \\
B_{v2} &= N_{v3} - C_{v_0}(\omega_{n_S}^2 + \omega_{n_F}^2 + 4\omega_{n_F}\omega_{n_S}\zeta_F\zeta_S) - C_{v_S}(2\omega_{n_F}\zeta_F + 2\omega_{n_S}\zeta_S) \\
B_{v3} &= N_{v4} - C_{v_0}(2\omega_{n_F}\zeta_F + 2\omega_{n_S}\zeta_S) - C_{v_S} \\
B_{v4} &= N_{v5} - C_{v_0}
\end{aligned}
$$

$$
\begin{Bmatrix} F_{v0} \\ S_{v0} \\ F_{v1} \\ S_{v1} \end{Bmatrix} = [\mathrm{CIM}] \begin{Bmatrix} B_{v1} \\ B_{v2} \\ B_{v3} \\ B_{v4} \end{Bmatrix}
$$

$$
\begin{aligned}
F_{v_{\mathrm{Cos}}} &= F_{v1} \\
S_{v_{\mathrm{Cos}}} &= S_{v1} \\
F_{v_{\mathrm{Sin}}} &= (F_{v0} - F_{v1}(-\sigma_F))/\omega_F \\
S_{v_{\mathrm{Sin}}} &= (S_{v0} - S_{v1}(-\sigma_S))/\omega_{\mathrm{S}}
\end{aligned}
$$

No-roll frame body z velocity coefficients:

$$
\begin{aligned}
N_{w0} &= B^2\delta + C^2\delta + 2AB\delta F + A^2\delta F^2 + 2AC\delta H + A^2\delta H^2 \\
N_{w1} &= -2AC\delta - \beta CF + B\delta F + A\delta F^2 + BFG + AF^2G + B^2\gamma + C^2\gamma \\
&\quad + 2ABF\gamma + A^2F^2\gamma + B\beta H - 2A^2\delta H + C\delta H + CGH + 2AC\gamma H + A\delta H^2 + AGH^2 + A^2\gamma H^2 \\
N_{w2} &= -B\beta + A^2\delta - C\delta - \alpha CF - CG + F^2G - 2AC\gamma + BF\gamma + AF^2\gamma + \alpha BH - 2A\delta H - 2AGH - 2A^2\gamma H + C\gamma H + GH^2 + A\gamma H^2 \\
&\quad - CD\tilde{q}_0 - ADH\tilde{q}_0 - BD\tilde{r}_0 - ADF\tilde{r}_0 - CD\tilde{q}_0 - ADH\tilde{q}_0 - BD\tilde{r}_0 - ADF\tilde{r}_0 + CF\tilde{v}_0 - BH\tilde{v}_0 + BF\tilde{w}_0 + AF^2\tilde{w}_0 + CH\tilde{w}_0 + AH^2\tilde{w}_0 \\
N_{w3} &= -\alpha B + A\delta + AG + A^2\gamma - C\gamma - 2GH - 2A\gamma H + AD\tilde{q}_0 - DH\tilde{q}_0 - DF\tilde{r}_0 + B\tilde{v}_0 - C\tilde{w}_0 + F^2\tilde{w}_0 - 2AH\tilde{w}_0 + H^2\tilde{w}_0 \\
N_{w4} &= G + A\gamma + D\tilde{q}_0 + A\tilde{w}_0 - 2H\tilde{w}_0 \\
N_{w5} &= \tilde{w}_0 \\
C_{w_S} &= \frac{N_{w0}}{\omega_{n_F}^2\omega_{n_S}^2} \\
C_{w_0} &= \frac{N_{w1} - C_{w_S}(2\omega_{n_S}\zeta_S\omega_{n_F}^2 + 2\omega_{n_F}\zeta_F\omega_{n_S}^2)}{\omega_{n_F}^2\omega_{n_S}^2} \\
B_{w1} &= N_{w2} - C_{w_0}(2\zeta_F\omega_{n_F}\omega_{n_S}^2 + 2\zeta_S\omega_{n_S}\omega_{n_F}^2) - C_{w_S}(\omega_{n_S}^2 + \omega_{n_F}^2 + 4\omega_{n_F}\omega_{n_S}\zeta_F\zeta_S) \\
B_{w2} &= N_{w3} - C_{w_0}(\omega_{n_S}^2 + \omega_{n_F}^2 + 4\omega_{n_F}\omega_{n_S}\zeta_F\zeta_S) - C_{w_S}(2\omega_{n_F}\zeta_F + 2\omega_{n_S}\zeta_S) \quad B_{w3} = N_{w4} - C_{w_0}(2\omega_{n_F}\zeta_F + 2\omega_{n_S}\zeta_S) - C_{w_S} \\
B_{w4} &= N_{w5} - C_{w_0} \quad \begin{Bmatrix} F_{w0} \\ S_{w0} \\ F_{w1} \\ S_{w1} \end{Bmatrix} = [\mathrm{CIM}] \begin{Bmatrix} B_{w1} \\ B_{w2} \\ B_{w3} \\ B_{w4} \end{Bmatrix} \quad F_{w_{\mathrm{Cos}}} = F_{w1} \quad S_{w_{\mathrm{Cos}}} = S_{w1} \quad F_{w_{\mathrm{Sin}}} = (F_{w0} - F_{w1}(-\sigma_F))/\omega_F \quad S_{w_{\mathrm{Sin}}} = (S_{w0} - S_{w1}(-\sigma_S))/\omega_{\mathrm{S}}
\end{aligned}
$$

No-roll frame body pitch rate coefficients:

$$Nq0 = 0$$

$$Nq1 = (B^2\delta + C^2\delta - A\beta CF + AB\delta F - B^2G - C^2G - ABFG + AB\beta H + AC\delta H - ACGH)/D$$

$$Nq2 = (-AB\beta - AC\delta - A\alpha CF - \beta CF + B\delta F + ACG - BFG + B^2\gamma + C^2\gamma + ABF\gamma + A\alpha BH + B\beta H + C\delta H - CGH + AC\gamma H - ACD\tilde{q}_0 - A^2DH\tilde{q}_0 - ABD\tilde{r}_0 - A^2DF\tilde{r}_0 + ACF\tilde{v}_0 - ABH\tilde{v}_0 - B^2\tilde{w}_0 - C^2\tilde{w}_0 - ABF\tilde{w}_0 - ACH\tilde{w}_0)/D$$

$$Nq3 = (-A\alpha B - B\beta - C\delta - \alpha CF + CG - AC\gamma + BF\gamma + \alpha BH + C\gamma H + A^2D\tilde{q}_0 - CD\tilde{q}_0 - 2ADH\tilde{q}_0 - BD\tilde{r}_0 - 2ADF\tilde{r}_0 + AB\tilde{v}_0 + CF\tilde{v}_0 - BH\tilde{v}_0 + AC\tilde{w}_0 - BF\tilde{w}_0 - CH\tilde{w}_0)/D$$

$$Nq4 = (-\alpha B - C\gamma + 2AD\tilde{q}_0 - DH\tilde{q}_0 - DF\tilde{r}_0 + B\tilde{v}_0 + C\tilde{w}_0)/D$$

$$Nq5 = \tilde{q}_0$$

$$C_{q_S} = \frac{N_{q0}}{\omega_{n_F}^2\omega_{n_S}^2}$$

$$C_{q_0} = \frac{N_{q1} - C_{q_S}(2\omega_{n_S}\zeta_S\omega_{n_F}^2 + 2\omega_{n_F}\zeta_F\omega_{n_S}^2)}{\omega_{n_F}^2\omega_{n_S}^2} \quad B_{q1} = N_{q2} - C_{q_0}(2\zeta_F\omega_{n_F}\omega_{n_S}^2 + 2\zeta_S\omega_{n_S}\omega_{n_F}^2) - C_{q_S}(\omega_{n_S}^2 + \omega_{n_F}^2 + 4\omega_{n_F}\omega_{n_S}\zeta_F\zeta_S)$$

$$B_{q2} = N_{q3} - C_{q_0}(\omega_{n_S}^2 + \omega_{n_F}^2 + 4\omega_{n_F}\omega_{n_S}\zeta_F\zeta_S) - C_{q_S}(2\omega_{n_F}\zeta_F + 2\omega_{n_S}\zeta_S) \quad B_{q3} = N_{q4} - C_{q_0}(2\omega_{n_F}\zeta_F + 2\omega_{n_S}\zeta_S) - C_{q_S}$$

$$B_{q4} = N_{q5} - C_{q_0} \begin{Bmatrix} F_{q0} \\ S_{q0} \\ F_{q1} \\ S_{q1} \end{Bmatrix} = [\mathrm{CIM}] \begin{Bmatrix} B_{q1} \\ B_{q2} \\ B_{q3} \\ B_{q4} \end{Bmatrix} \quad F_{q_{\mathrm{Cos}}} = F_{q1} \quad S_{q_{\mathrm{Cos}}} = S_{q1} \quad F_{q_{\mathrm{Sin}}} = (F_{q0} - F_{q1}(-\sigma_F))/\omega_F \quad S_{q_{\mathrm{Sin}}} = (S_{q0} - S_{q1}(-\sigma_S))/\omega_S$$

No-roll frame body yaw rate coefficients:

$$Nr0 = 0 \quad Nr1 = (-B^2\beta - \beta C^2 - AB\beta F - AC\delta F + ACFG - A\beta CH + AB\delta H - ABGH)/D$$

$$Nr2 = (-\alpha B^2 + A\beta C - \alpha C^2 - AB\delta - A\alpha BF - B\beta F - C\delta F + ABG + CFG - ACF\gamma - A\alpha CH - \beta CH + B\delta H - BGH + AB\gamma H + ABD\tilde{q}_0 + A^2DF\tilde{q}_0 - ACD\tilde{r}_0 - A^2DH\tilde{r}_0 + B^2\tilde{v}_0 + C^2\tilde{v}_0 + ABF\tilde{v}_0 + ACH\tilde{v}_0 + B^2\tilde{v}_0 + C^2\tilde{v}_0 + ABF\tilde{v}_0 + ACH\tilde{v}_0 + ACF\tilde{w}_0 - ABH\tilde{w}_0)/D$$

$$Nr3 = (A\alpha C + \beta C - B\delta - \alpha BF + BG - AB\gamma - CF\gamma - \alpha CH + B\gamma H + BD\tilde{q}_0 + 2ADF\tilde{q}_0 + A^2D\tilde{r}_0 - CD\tilde{r}_0 - 2ADH\tilde{r}_0 - AC\tilde{v}_0 + BF\tilde{v}_0 + CH\tilde{v}_0 + AB\tilde{w}_0 + CF\tilde{w}_0 - BH\tilde{w}_0)/D$$

$$Nr4 = (\alpha C - B\gamma + DF\tilde{q}_0 + 2AD\tilde{r}_0 - DH\tilde{r}_0 - C\tilde{v}_0 + B\tilde{w}_0)/D \quad Nr5 = \tilde{r}_0 \quad C_{r_S} = \frac{N_{r0}}{\omega_{n_F}^2\omega_{n_S}^2} \quad C_{r_0} = \frac{N_{r1} - C_{r_S}(2\omega_{n_S}\zeta_S\omega_{n_F}^2 + 2\omega_{n_F}\zeta_F\omega_{n_S}^2)}{\omega_{n_F}^2\omega_{n_S}^2}$$

$$B_{r1} = N_{r2} - C_{r_0}(2\zeta_F\omega_{n_F}\omega_{n_S}^2 + 2\zeta_S\omega_{n_S}\omega_{n_F}^2) - C_{r_S}(\omega_{n_S}^2 + \omega_{n_F}^2 + 4\omega_{n_F}\omega_{n_S}\zeta_F\zeta_S) B_{r2} = N_{r3} - C_{r_0}(\omega_{n_S}^2 + \omega_{n_F}^2 + 4\omega_{n_F}\omega_{n_S}\zeta_F\zeta_S)$$

$$- C_{r_S}(2\omega_{n_F}\zeta_F + 2\omega_{n_S}\zeta_S) \quad B_{r3} = N_{r4} - C_{r_0}(2\omega_{n_F}\zeta_F + 2\omega_{n_S}\zeta_S) - C_{r_S} \quad B_{r4} = N_{r5} - C_{r_0} \begin{Bmatrix} F_{r0} \\ S_{r0} \\ F_{r1} \\ S_{r1} \end{Bmatrix} = [\mathrm{CIM}] \begin{Bmatrix} B_{r1} \\ B_{r2} \\ B_{r3} \\ B_{r4} \end{Bmatrix} \quad F_{r_{\mathrm{Cos}}} = F_{r1}$$

$$S_{r_{\mathrm{Cos}}} = S_{r1} \quad F_{r_{\mathrm{Sin}}} = (F_{r0} - F_{r1}(-\sigma_F))/\omega_F \quad S_{r_{\mathrm{Sin}}} = (S_{r0} - S_{r1}(-\sigma_S))/\omega_S$$

Projectile pitch orientation coefficients:

$$F_{\theta_{\mathrm{Cos}}} = D/V(F_{q_{\mathrm{Cos}}}\sigma_F - F_{q_{\mathrm{Sin}}}\omega_F)/\omega_{n_F}^2 \quad F_{\theta_{\mathrm{Sin}}} = D/V(F_{q_{\mathrm{Sin}}}\sigma_F + F_{q_{\mathrm{Cos}}}\omega_F)/\omega_{n_F}^2 \quad S_{\theta_{\mathrm{Cos}}} = D/V(S_{q_{\mathrm{Cos}}}\sigma_S - S_{q_{\mathrm{Sin}}}\omega_S)/\omega_{n_S}^2$$

$$S_{\theta_{\mathrm{Sin}}} = D/V(S_{q_{\mathrm{Cos}}}\sigma_S + S_{q_{\mathrm{Sin}}}\omega_S)/\omega_{n_S}^2 \quad C_{\theta_S} = \left(\frac{D}{V}\right)C_{q_0} \quad C_{\theta_{SS}} = 1/2\left(\frac{D}{V}\right)C_{q_S} \quad C_{\theta_0} = \theta_0 - F_{\theta_{\mathrm{Cos}}} - S_{\theta_{\mathrm{Cos}}}$$

Projectile yaw orientation coefficients:

$$F_{\psi_{\mathrm{Cos}}} = D/V(F_{r_{\mathrm{Cos}}}\sigma_F - F_{r_{\mathrm{Sin}}}\omega_F)/\omega_{n_F}^2 \quad F_{\psi_{\mathrm{Sin}}} = D/V(F_{r_{\mathrm{Cos}}}\sigma_F + F_{r_{\mathrm{Sin}}}\omega_F)/\omega_{n_F}^2 \quad S_{\psi_{\mathrm{Cos}}} = D/V(S_{r_{\mathrm{Cos}}}\sigma_S - S_{r_{\mathrm{Sin}}}\omega_S)/\omega_{n_S}^2$$

$$S_{\psi_{\mathrm{Sin}}} = D/V(S_{r_{\mathrm{Cos}}}\sigma_S + S_{r_{\mathrm{Sin}}}\omega_S)/\omega_{n_S}^2 \quad C_{\psi_S} = \left(\frac{D}{V}\right)C_{r_0} \quad C_{\psi_{SS}} = 1/2\left(\frac{D}{V}\right)C_{r_S} \quad C_{\psi_0} = \psi_0 - F_{\psi_{\mathrm{Cos}}} - S_{\psi_{\mathrm{Cos}}}$$

Projectile cross-range position coefficients:

$$F_{y_{\mathrm{Cos}}} = (D(F_{\psi_{\mathrm{Cos}}}\sigma_F - F_{\psi_{\mathrm{Sin}}}\omega_F) + D/V(F_{v_{\mathrm{Cos}}}\sigma_F - F_{v_{\mathrm{Sin}}}\omega_F))/\omega_{n_F}^2 \quad F_{y_{\mathrm{Sin}}} = (D(F_{\psi_{\mathrm{Cos}}}\omega_F + F_{\psi_{\mathrm{Sin}}}\sigma_F) + D/V(F_{v_{\mathrm{Cos}}}\omega_F + F_{v_{\mathrm{Sin}}}\sigma_F))/\omega_{n_F}^2$$

$$S_{y_{\mathrm{Cos}}} = (D(S_{\psi_{\mathrm{Cos}}}\sigma_S - S_{\psi_{\mathrm{Sin}}}\omega_S) + D/V(S_{v_{\mathrm{Cos}}}\sigma_S - S_{v_{\mathrm{Sin}}}\omega_S))/\omega_{n_S}^2 \quad S_{y_{\mathrm{Sin}}} = (D(S_{\psi_{\mathrm{Cos}}}\omega_S + S_{\psi_{\mathrm{Sin}}}\sigma_S) + D/V(S_{v_{\mathrm{Cos}}}\lambda_{SI} + S_{v_{\mathrm{Sin}}}\sigma_S))/\omega_{n_S}^2$$

$$C_{y_S} = (D)C_{\psi_0} + \left(\frac{D}{V}\right)C_{v_0} \quad C_{y_{SS}} = \frac{1}{2}(D)C_{\psi_S} + \frac{1}{2}\left(\frac{D}{V}\right)C_{v_S} \quad C_{y_{SSS}} = \frac{1}{3}(D)C_{\psi_{SS}} \quad C_{y_{0_n}} = Y_{cg_0} - F_{y_{\mathrm{Cos}}} - S_{y_{\mathrm{Cos}}}$$

Projectile vertical position coefficients:

$$F_{z_{\mathrm{Cos}}} = (D/V(F_{w_{\mathrm{Cos}}}\sigma_F - F_{w_{\mathrm{Sin}}}\omega_F) - D(F_{\theta_{\mathrm{Cos}}}\sigma_F - F_{\theta_{\mathrm{Sin}}}\omega_F))/\omega_{n_F}^2 \quad F_{z_{\mathrm{Sin}}} = (D/V(F_{w_{\mathrm{Sin}}}\sigma_F + F_{w_{\mathrm{Cos}}}\omega_F) - D(F_{\theta_{\mathrm{Sin}}}\sigma_F + F_{\theta_{\mathrm{Cos}}}\omega_F))/\omega_{n_F}^2$$

$$S_{z_{\mathrm{Cos}}} = (D/V(S_{w_{\mathrm{Cos}}}\sigma_S - S_{w_{\mathrm{Sin}}}\omega_S) - D(S_{\theta_{\mathrm{Cos}}}\sigma_S - S_{\theta_{\mathrm{Sin}}}\omega_S))/\omega_{n_S}^2 \quad S_{z_{\mathrm{Sin}}} = (D/V(S_{w_{\mathrm{Sin}}}\sigma_S + S_{w_{\mathrm{Cos}}}\omega_S) - D(S_{\theta_{\mathrm{Sin}}}\sigma_S + S_{\theta_{\mathrm{Cos}}}\omega_S))/\omega_{n_S}^2$$

$$C_{z_S} = \left(\frac{D}{V}\right)C_{w_0} - (D)C_{\theta_0} \quad C_{z_{SS}} = \frac{1}{2}\left(\frac{D}{V}\right)C_{w_S} - \frac{1}{2}(D)C_{\theta_S} \quad C_{z_{SSS}} = -\frac{1}{3}(D)C_{\theta_{SS}} \quad C_{z_{0n}} = Z_{cg_0} - F_{z_{\mathrm{Cos}}} - S_{z_{\mathrm{Cos}}}$$

References

[1] *Field Manual 23-10: Sniper Training*, U.S. Army, Washington, D.C., 1994, pp. 3-29–3-35.

[2] Bucco, D., *An Improved Algorithm for Artillery Fire Control*, Dept. of Defense, Weapons Systems Research Lab., Adelaide, Australia, 1983, pp. 1–69.

[3] Breaux, H. J., "A Methodology for the Development of Fire Control Equations for Guns and Rockets Fired from Aircraft," *Transactions of the 2nd Army Conference on Applied Mathematics and Computing*, Washington, D.C., May 1984.

[4] McCoy, R., *Modern Exterior Ballistics*, Schiffer Publ., Atglen, PA, 1999, pp. 165–183, 240–244.

[5] Hainz, L., and Costello, M., "Modified Projectile Linear Theory for Rapid Trajectory Prediction," *Journal of Guidance, Control, and Dynamics*, Vol. 28, No. 5, 2005, pp. 1006–1014.
doi:10.2514/1.8027

[6] Costello, M., and Peterson, A., "Linear Theory of a Dual-Spin Projectile in Atmospheric Flight," *Journal of Guidance, Control, and Dynamics*, Vol. 23, No. 5, 2000, pp. 789–797.
doi:10.2514/2.4639

[7] Frost, G., and Costello, M., "Linear Theory of a Projectile with a Rotating Internal Part in Atmospheric Flight," *Journal of Guidance, Control, and Dynamics*, Vol. 27, No. 5, 2004, pp. 898–906.
doi:10.2514/1.1115

[8] McCoy, R. L., "The Effect of Wind on Flat-Fire Trajectories," Ballistic Research Lab., Rept. 1900, Aberdeen Proving Ground, MD, 1976.

[9] Ollerenshaw, D., and Costello, M., "Model Predictive Control of a Direct Fire Projectile Equipped with Canards," *Journal of Dynamic Systems, Measurement, and Control*, Vol. 130, No. 6, 2008, p. 061010.
doi:10.1115/1.2957624

[10] Costello, M., and Rogers, J., "Boom: A Computer Aided Engineering Tool for Exterior Ballistics of Smart Projectiles," U.S. Army Research Lab. CR-670, June 2011.

J. How
Associate Editor